Multi-parametric, label-free and non-contact approach to bacteria single-cells and biofilm formation detection

Igor Buzalewicz[1], Agnieszka Ulatowska-Jarza[1], Marlena Gąsior-Głogowska[1], Mirela Wolf-Baca[2], Pawel Zylka[3]

e-mail: agnieszka.ulatowska-jarza@pwr.edu.pl, marlena.gasior-glogowska@pwr.edu.pl, mirela.wolf-baca@pwr.edu.pl, igor.buzalewicz@pwr.edu.pl, pawel.zylka@pwr.edu.pl

[1] Department of Biomedical Engineering, Faculty of Fundamental Problems of Technology, Wroclaw University of Science and Technology, 27 Wybrzeze S. Wyspianskiego St., 50-370 Wroclaw, Poland

[2]Department of Environmental Protection Engineering, Faculty of Environmental Engineering, Wroclaw University of Science and Technology, 27 Wybrzeze S. Wyspianskiego St., 50-370 Wroclaw, Poland

[3] Department of Electrical Engineering Fundamentals, Wroclaw University of Science and Technology, 27 Wybrzeze S. Wyspianskiego St., 50-370 Wroclaw, Poland

*corresponding author: igor.buzalewicz@pwr.edu.pl

Abstract

Understanding the mechanism of biofilm formation is essential to progress in the field of microbiology and infection control. Here we demonstrate a new approach to detect bacterial single cell and biofilms using label-free and non-contact methods. Multimode measurements using Kelvin probe, digital holographic tomography and infrared microscopy were performed on *E. coli* cells. The proposed analysis provides the multi-parametric detection of bacteria based on contact potential difference, refractive index data and infrared spectra related to electrical, optical, morphological, and chemical properties of the single cells. Moreover, it is the first attempt to use the Kelvin Probe and contact potential difference measurements for bacteria sensing. The obtained results confirmed that it is possible to use the mentioned above techniques for examination of the biofilm formation. Furthermore, it was confirmed that after only 24 hours *E. coli* bacteria formed biofilm on the analyzed surfaces without the presence of any nutrients.

Keywords: Kelvin Probe, Contact Potential Difference, Digital Holographic Tomography, Infrared Microscopy, Bacteria, Single-Cells, Biofilm Formation

Highlights

- Multi-parametric label-free sensing of the biofilm formation on different surfaces.
- Suitable method for transparent/ non-transparent, conducting/semi- or non-conducting materials.
- Multi-mode large-scale examination by Kelvin probe, Holotomography and IR - microscopy
- Contact Potential Difference measurement for detection of biofilm development.
- Confirmation of biofilm formation on glass and stainless steel after 24 hours.

1. INTRODUCTION

The technological developments are omnipresent and becoming more and more applied in our everyday life. The devices that historically have been used in particular application became multifunctional products. The phones, which were used for verbal communications, have advanced with the development of the wireless technology, and apart from its primary function became our cameras, data storage, wallets, social life centers and health monitors. Mobile solutions are revolutionizing the modern medicine, as the collection, hosting and managing of relevant data became accessible, easy, paper free and manageable.

The advancement in remote medicine has made a substantial impact during the world-wide Covid-19 pandemic. Patients have been offered consultations over mobile phones or videos, but also where relevant, equipped with innovative telehealth and telecare products in the form of a personal digital assistant. Mobile communication devices used as medical devices have an extremely useful way of communication and exchange of the information between patients and healthcare providers, including hospitals, supporting some aspects of clinical diagnosis and education. The benefits of mobile devices are boundless, but there is a growing concern around the potential contamination of their surfaces [1,2]. The transmission of microbial infections during epidemics and pandemics through surface contamination became a public awareness from the beginning of the Covid-19 pandemic, and uncovered the relevance of the disinfection practices that can be available to everyone [3], as the pathogens colonize the surfaces and in consequence lead to increased transmission of infections. The cleaning regime is relevant for all medical devices, as the microorganisms attach to a surface, produce extracellular polymers, which promote further attachment and in consequence formation of clinically relevant biofilm. The presence of biofilm contributes to a decreased susceptibility of the microorganism to disinfectants, and therefore creating a significant bioburden for public health.

The most common way of removing pathogens from the medical surfaces of is sterilization through steam or radiation or chemical treatment. These procedures are usually not suitable for the devices that have electronic components, but also, they are not widely available to the society. In example, people who live with diabetes require frequent control of the sugar levels, which are usually provided by inexpensive glucometers in long-term care facilities. There is a wide range of glucometers used at the various facilities and each has its own cleaning requirements per the manufacturer [4]. In cases where the manufacturer does not provide any cleaning recommendations, use of e.g. an EPA-registered high-level disinfectant is the standard [5]. However, inappropriate disinfection may lead to increase of the microorganisms' transmission and in consequence infection rate within the facility. To reduce bacterial contamination risks time intervals between decontamination must be identified and regular decontamination of mobile communication devices must be performed, along with ensuring proper patient education on hand hygiene [6].

The meta-analysis on the dissemination of pathogens and studies to identify effective prevention measures was already reported [7]. It was found that only 8% of healthcare workers routinely cleaned their mobile communication devices resulting in a rate of contamination between 40% and 100%. Coagulase-negative Staphylococci and *Staphylococcus aureus* (*S. aureus*) were the most common bacteria with 10 up to 95.3% proportion of them were Methicillin-resistant *S. aureus* (MRSA). Another review reported microbial presence on mobile phones in both health care and community settings [8]. A total of 56 studies from 24 countries were included in the review. In 54 out of 56 sources the presence of bacteria was confirmed along 16 studies also reported presence of fungi. *S. aureus* and coagulase-negative Staphylococci were the most frequent organisms identified on mobile phones. These two species along with *Escherichia coli* (*E. coli)* were present in over a third of studies both in health care and community samples. MRSA*, Acinetobacter* sp., and *Bacillus* sp. were present in over a third of the studies in health care settings only. The *E. coli (*and *Streptococci sp*) are the first bacteria to colonize the gastrointestinal tract of humans upon birth, paving the way for the establishment of species of the *Bifidobacterium*, *Bacteroides* and other genera [9].

Application of mobile devices in healthcare is becoming an integral part of modern medicine, with a potential global public health risk for microbial transmission. The aim of the presented studies was to perform a multi-mode examination on the potential role of glass display as well as a metallic cover of the mobile communication devices in the occurrence of bacterial biofilms formed by *E. coli*. The specific purpose was to indicate how long it will take for bacteria to colonize relatively smooth surfaces and to easily detect the colonization. The *E. coli* was selected as a well-established model organism for the study of surface bacterial colonization.

The *E. coli* colonization was carried out on stainless steel and glass surfaces, as these two materials are commonly used in mobile devices, with longer life-span comparing to plastic surfaces. The innovative approach to bacteria and biofilm detection was applied, where multimodal measurement techniques such as Kelvin probe, infrared spectroscopy, and digital holographic tomography.

Kelvin probe is a non-contact, capacitively coupled voltage measuring technique capable of sensing low (typically up to a few volts) potential differences between the probe conductive tip and the analyzed material surface directly beneath the probe. It is referred to as a Contact Potential Difference (CPD) or Surface Potential (SP). CPD results from a dissimilarity in the Work Function (WF) of the probe tip metal and the examined material and it is thus very sensitive to any surface contamination or changes in its chemical composition. The method was originally established by lord Kelvin [10], technologically advanced by Zisman to use ac modulation technique [11] and recently adopted by Baikie to use off-null detection method in Scanning Kelvin Probe (SKP) [12] providing linear profiles and 2D maps of the CPD and WF distribution in large (tens of mm) regions [13]. Although theoretical foundations of using off-null detection SKP in biological tissue analysis have been laid down [14], no literature evidence has been found so far for its use to study attachment of bacteria and biofilm growth in large specimen surface regions. Kelvin probe attachment is also commonly used in Atomic Force Microscopy (AFM) developing Kelvin Probe Force Microscopy (KPFM) known also as Scanning Surface Potential Microscopy (SSPM). Although it is a truly valuable research tool of nanometer three-dimensional resolution, it offers very narrow spatial region to be explored (tens of μm) and moreover, it is still discussable whether it can provide a true contact potential difference (and thus WF) not obscured by the atomic-scale tip-object distance and the resulting local distortion of the energy bands altering WF values [15]. Yet, KPFM has been successively applied to map the micro-scale distribution and provide insight into the attachment process of *P. aeruginosa* and *S. aureus* on Au and stainless steel surfaces [16], adhesion of single *B. thuringiensis* and *B. anthracis* spores to solid Au, Si and mica surfaces [17] or microscale inhibition of bacterial adhesion and further biofilm formation on polymeric surfaces covered with antimicrobial bromohexane N-alkylated polyethyleneimine brushes [18], just to name a few its bacteria-related scientific applications.

Fourier transform infrared microscopy (μFTIR) was used to confirm the presence of biofilm formation on the stainless-steel surfaces. This vibrational spectroscopic technique is a powerful tool for bacterial analysis, enabling direct detection, identification and classification of microorganisms [19–21]. Moreover, it is widely used to study the biochemical composition of biofilm produced by various bacteria [22,23]. μFTIR allows the investigation of the spatial distribution of proteins, lipids and polysaccharides, providing a two dimensional map of the absorption as a function of wavenumber throughout the sample surface. The appearance of bacterial typical signals, such as strong absorbance in the nucleic acid and polysaccharide region (1200-900 cm^{-1}) [24], is a strong evidence of the existence of *E. coli* cells on the studied surface. μFTIR has been also demonstrated as bacterial viability assessment method [25], allowing discrimination between living and death cells.

The evaluation and confirmation of the bacterial biofilm and formation on the glass surface the digital holographic tomography (DHT), which is suitable for non-contact and non-destructive 3D optical imaging of single cells, was applied. In DHT based on the limited-angle holographic tomography [26–28], the series of digital holograms is registered at various incident angles of the illumination beam. Based on the principles of optical diffraction tomography, it is possible to reconstruct 3D refractive index (RI) tomograms of optically transparent objects by interferometric, tomographic (at various illumination angles) imaging [29,30]. The provided RI-data are directly related with the local changes of the intracellular density, particularly protein density, what can be used for quantitative phenotyping of living, unlabeled cells. DHT is label-free, non-invasive, fast and high-resolution technique being an alternative to the microscopic techniques: scanning confocal fluorescence microscopy or 2D imaging techniques as fluorescence microscopy, or phase contrast and differential interference contrast microscopy, commonly used in biology and biomedical applications. Recently, there have been many reports on the application potential of this technique, including for example studies on: hematology [31], oncology [32], cell biology [33,34], neuroscience [35], drug discovery [36], microbiology etc.

2. MATERIALS AND METHODS

2.1. Substrates

A medical- and food-grade stainless steel (grade 316L, UNS S31603) was selected as a model metallic substrate. Round specimens (16 mm in diameter) machined directly of a 0,5 mm thick flat sheet metal were grinded using super fine (2500 grit) sandpaper to obtain average roughness R_z=1.25 μm +/-0.98 μm (verified using roughness tester Mitutoyo SurfTest SJ-210). The specimens were then ultrasonically cleaned in distilled water, acetone, absolute ethanol (both analytical grade) and distilled water again (15 min in each bath), naturally dried and stored in clean laboratory air to naturally re-passivate their surface. One half of the specimen surface was subsequently masked using pressure-sensitive polysiloxane self-adhesive polyimide film (70110, PPI Adhesive Products Ltd.) as illustrated in Figure 1.

To examine the biofilm formation on glass surfaces the glass-bottom micro-dishes (μ-Dish 35 mm low, Ibidi, Germany; average glass surface roughness R_z=0.094 μm +/-0.019 μm) were used. In order to avoid external bacterial contamination, all stainless steel specimens masked with 70110 tape as well as glass micro-dishes were sterilized in an autoclave at 121°C for 20 minutes prior to biofilm culture.

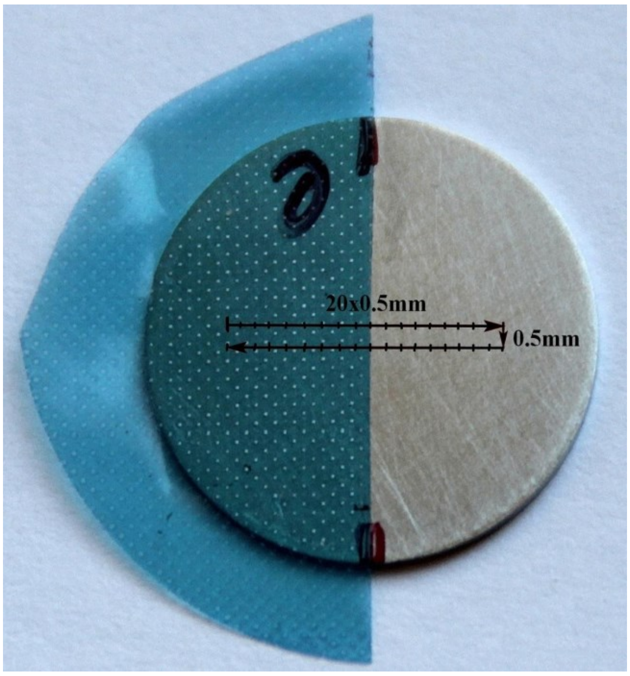

Figure 1. Stainless steel specimen masked with 70110 tape (with schematically outlined path along which the Kelvin probe was relocated in line scan).

2.2. Bacterial suspension

A reference strain of *Escherichia coli* (E.coli) ATCC® 2592 bacteria (BioMaxima) was used for this study. A bacterial suspension was prepared from a 24 hours culture at a density of 0.5 McFarland ($1.5*10^8$ CFU/ml) (BioMaxima). Each stainless steel and glass-surface specimen was placed in a sterile flask in 100 ml of nutrient agar (BTL) inoculated with 1ml of standard strain. The whole was kept under continuous stirring on a shaker (Elpin, 180 rpm) at 37°C. Biofilm-covered steel and glass-surface specimens were disassembled after 24 and 72 hours respectively and excess medium was washed off with sterile distilled water (5ml). Each specimen was then resuspended in 100 µl of sterile water and stored in a refrigerator (4°C) for further analysis, which was carried out generally in 1-3 hours. Reference stainless steel specimens were prepared in an analogous way however, in this case the nutrient agar was not inoculated with bacterial suspension. The 5 specimens of biofilm as well as 5 reference specimens were prepared for each incubation time duration.

2.3. SEM topography analysis

The 316L stainless steel specimens bred for 24 hours in bacteria-agar suspension were also prepared for SEM analysis; in this case they were passively desiccator-dried for 7 days and analyzed without any additional metallization. Surface microtopography analysis was performed using Scanning Electron Microscope (SEM) (Ga-FIB Helios NanoLab™ 600i, FEI) fitted with EDT detector and operated at low 2.0 kV accelerating voltage (corresponding to 0.17 nA electron beam current) in order not to destroy bacterial substance. Basic SEM image analysis was performed using ImageJ software (ver. 1.53e) package and its image binarization and particle analysis macros.

2.4. Scanning Kelvin probe

An environmental Scanning Kelvin probe (SKP) with off-null detection system (SKP5050, KP Technology, Scotland) was used for all CPD measurements. The probe oscillator was supplied at 40 a.u. and 67.0 Hz, the probe backing voltage V_b (routed to the probe tip) was varied between +/- 5.0 V, $4x10^7$ V/A current gain and tenfold signal averaging was applied while the gradient was maintained at 200 a.u. by the off-null system detection algorithm. A stainless-steel probe tip (supplied by the SKP manufacturer) with a diameter of 1 mm was used. The probe tip was cleaned with absolute ethyl alcohol and air-dried before operation. Stainless steel specimens encrusted with *E. coli* biofilm were rinsed by dipping them in distilled water and gently air-dried. The masking tape was then unpeeled, and the samples were fixed on a mobile SKP apparatus stage. CPD measurements were performed under laboratory conditions (temperature 21-24°C, humidity 30-40% RH) as 10 mm long line scans as well as 10x10 mm 2D scans (with 0.5 mm increments) traversing the center of the specimen. CPD measurement conditions allow to estimate the effective area observed by the Kelvin probe as ca. 1 mm^2. Therefore, CPD determined at a single point along a scanline (and in 2D maps) corresponded to the average value over the area of 1 mm^2 under the probe tip. The calibration step was performed using Au-evaporated reference specimen to calculate WF of the probe tip material WF_{tip}.

The recorded data was averaged and statistically analyzed (using Shapiro-Wilk and Kolmogorov-Smirnov normality test as well as 1 way ANOVA) at 95 % confidence interval.

2.5. μFTIR evaluation

Nicolet iN10 MX FTIR microscope (Thermo Scientific Inc., USA) equipped with a liquid nitrogen cooled MCT-A detector and a germanium Slide-On Ge Micro-Tip ATR accessory was used to spatially map out the surface constituents of the analyzed stainless steel specimen with bacterial film as well as the reference bacteria-free specimen region (i.e. masked with polyimide film during bacteria culture). The FTIR microscope was continuously purged with dry air. The 10x10 maps were collected with the rectangular aperture array of 50×50 μm^2 with spatial resolution of 50 μm (thus, 0.5 x 0.5 mm area of the specimen was scanned). Each spectrum was recorded in the range of 4000–650 cm^{-1} at a spectral resolution of 4 cm^{-1} and with 128 or 512 accumulated scans for samples and the background, respectively.

Data analysis was carried out using the Omnic and Omnic Picta software (Thermo Scientific Inc., USA) and OriginPro 2019 program (OriginLab Corporation, USA). The spectra preprocessing included: baseline corrections and smoothing with the Savitzky-Golay filter (parameters: polynomial order 2, window 35 [37]).

2.6. Digital holographic tomographic examination

The commercial off-axis Mach–Zehnder interferometric setup with a rotatable scanning mirror (3D Cell Explorer, Nanolive, Switzerland) was used. The series of digital holograms were registered at the 520 nm wavelength by dry microscope objective (60×, numerical aperture NA=0.8, Nikon) for each position of the scanning mirrors on rotatable arm of interferometer. The reconstruction of digital holograms, 3D-RI tomograms and rendered 3D visualizations of bacteria cells were performed by STEVE software (Nanolive, Switzerland). Each 3D-RI tomogram contains 95 slices (2D-RI tomograms). The digital staining of the single bacteria cells was performed based on the reconstructed 3D-RI distribution, which enables the visualization of the single bacteria cells present in the examined sample by determining the range of RI-values corresponding to the volume of the bacteria cells.

3. RESULTS AND DISCUSSION

3.1 SEM imaging of E. coli-encrusted 316L steel surface

Figure 2 A shows an exemplary low-magnification (x100) surface topography of 316L stainless steel specimen bred for 24 hours in *E. coli* bacterial suspension. Even though the breed time was relatively short the specimen surface has become irregularly encrusted with bacterial colonies at average surface coverage factor 0.6 %, median surface area 48 μm^2. They colonies were localized mainly in surface crevices or near other steel face defects or irregularities as it is evidenced in Figure 2 B. This can be related to the increased surface roughness within these areas, which could have influenced ability of the bacteria to attach to the surface [38]. Dehydrated bacteria displayed a regular rod-like shape with 1.6 μm length and 0.4 μm width on average. The mean dimensions recorded for the air-dried *E. coli* cells compare well with those reported in the literature [39].

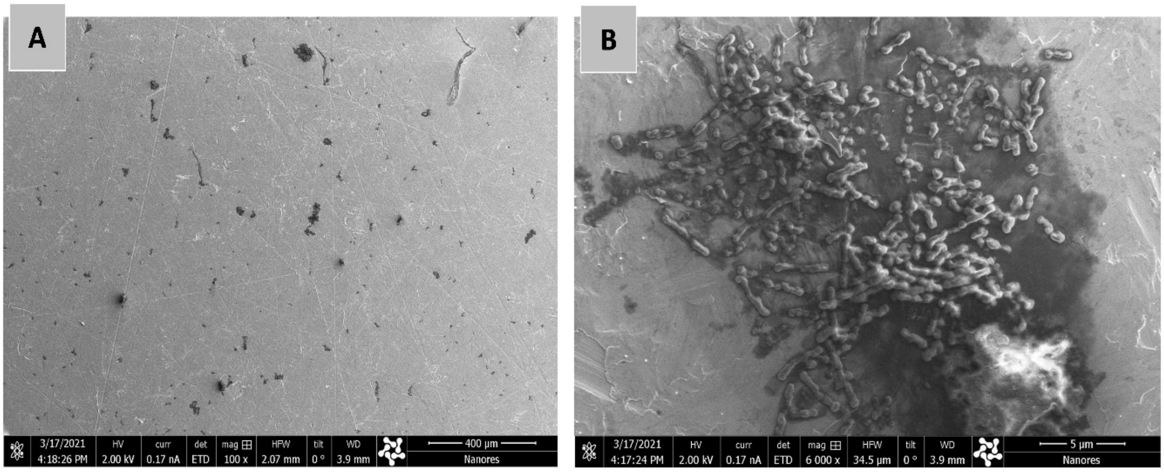

Figure 2. Surface topography of 316L stainless steel specimen bred for 24h in bacterial suspension: (A) 2 x 1.4 mm surface region, (B) *E. coli* biofilm structure (original SEM images, unprocessed).

3.2 CPD scans

In order to calculate WF of the probe tip material WF_{tip} a calibration was performed using Au-evaporated reference specimen, as shown in Figure 3 A. The mean value of the CPD recorded between the probe tip and Au reference surface amounted to +0.378 +/-0.032 V. Therefore, as the work function of gold WF_{Au} may be assumed to vary between 5.16 eV and 5.33 eV [12] thus WF_{tip} remains within 4.78-4.95 eV range which perfectly agrees with values 4.76-4.96 eV provided in literature for polycrystalline 316L stainless steel [13]. Thus, the mean value of the WF_{tip}=4.87 eV was adopted for further CPD measurement data processing as the 1 mm in diameter SKP probe tip inherently averages crystal grain-related local WF variations. CPD spatial distribution of exemplary tape-masked 316L stainless steel specimen dipped for 24h in distilled water was shown in Figure 3 B. Statistical analysis of such specimens revealed the mean CPD=+143 mV for 24h H_2O-dipped 316L steel material, (corresponding to the mean WF = 5.01 eV) while for specimens immersed for 72h the mean CPD = +130 mV (corresponding to WF = 4.91 eV). Both CPD values were statistically different (as evaluated using ANOVA 1 way test) thus the 72h-long water dipping of 316L stainless resulted in statistically meaningful change of its WF although the dissimilarity of the WF registered in this period was equal to 0.1 eV i.e. it was smaller than 2% of its initial value. This minor change in WF was related to slow electrochemical-in-origin oxidation of the 316L steel surface by H_2O and the resulting emergence of Fe and Cr oxide and peroxide precipitates which formed a moderately-conducting barrier film passivating the steel surface [40].

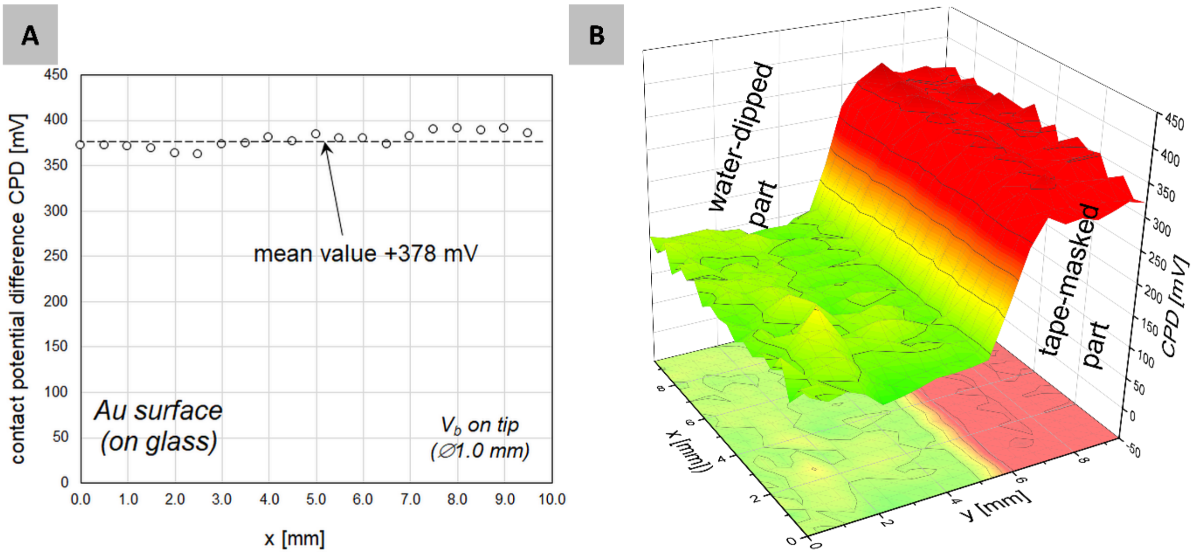

Figure 3. Exemplary CPD distribution: (**A**) along Au reference surface, (**B**) for tape-masked 316L stainless steel specimen dipped in distilled water for 24 hours.

The analysis performed for the tape-masked fragments of the 316L steel specimens showed that 24 hours-long contact with the masking tape resulted in the mean CPD=+360 mV while 72 hours-long period increased its CPD to +399mV. Those two CPD values were statistically different thus the contact with the polysiloxane adhesive of the masking tape changed the CPD of the 316L steel and the prolonged 72 hours-long exposure was shifting CPD towards higher values (although an exact dependency of the CPD shift with time was not evaluated as it was not within the scope of the current study). Thus, it suggests that some remains of the polysiloxane adhesive were present on the steel surface after peeling the tape off, as it has been discussed further in the manuscript section related to µFTIR analysis. Moreover, the analysis indicates that the CPD of the 316L specimen part screened out with the siloxane adhesive tape is not suitable as an invariable reference value.

Fig. 4 illustrates exemplary CPD variations in 316L stainless steel specimen half-masked with 70110 tape and encrusted with *E.coli* bred for 24 and 72 hours respectively. The mean CPD (averaged among all examined specimens) in the part encrusted with *E. coli* bred for 24h and 72h yields +57 mV and +7 mV respectively and were statistically different. On the other hand, the mean CPD of the reference 316L steel specimens retained in bacteria-free agar for 24h and 72h yielded -56 mV and -15 mV respectively.

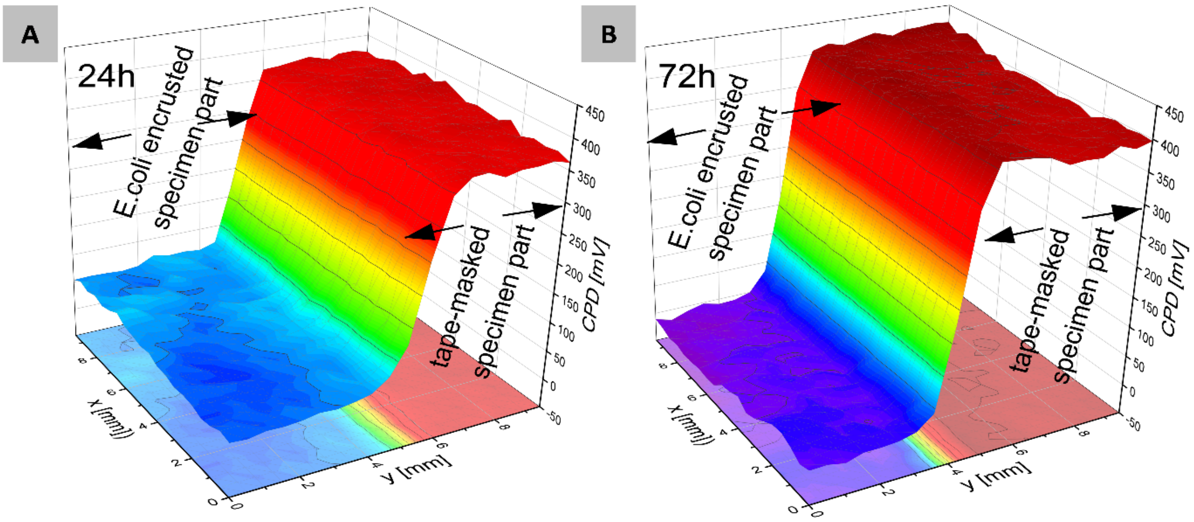

Figure 4. Exemplary CPD distribution in 316L stainless steel specimen half-masked with PPI tape and encrusted with *E. coli* cultivated for: (**A**) 24h, (**B**) 72h.

Thus, not only the mean CPD values of the bacterial films bred for 24h and 72h were statistically different from each other but they were also statistically different from the corresponding reference specimens produced in bacteria-free agar. The mean CPD of the specimens covered with bacterial film were also statistically different from the mean CPD values recorded for specimens dipped in distilled water.

The above findings were graphically summarized in the box chart shown in Figure 5, which was additionally scaled with WF values for comparison purposes. While the mean CPD of the 316L specimens kept in bacteria-free agar was rising with the retention time, the mean CPD of the bred-time corresponding bacterial films was declining as the biofilm breed time was prolonged. Thus, the presence of the bacterial colonies on the 316L steel specimen surface not only charged its CPD but also significantly altered its time evolution.

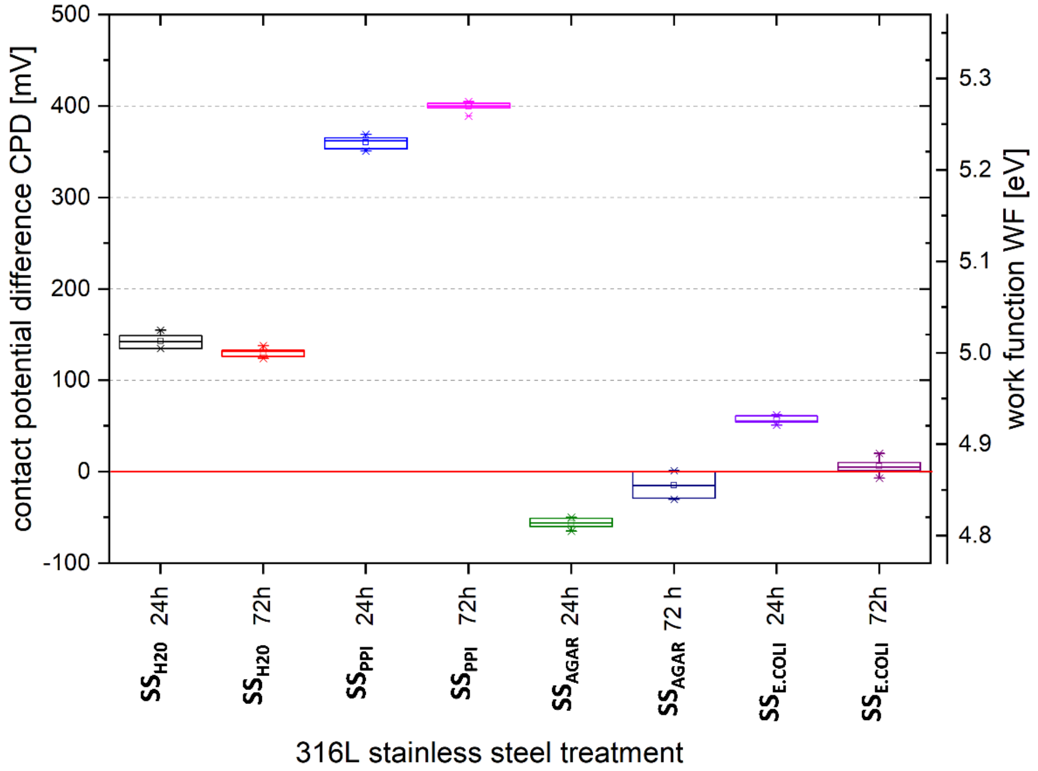

Figure 5. Statistical CPD variations in 316L stainless steel (SS) specimens undergoing different treatments, where 24h and 72h indicate treatment duration, SS_{H2O} denotes water dipping, SS_{PPI} symbolizes tape-masking, SS_{AGAR} indicates reference specimens prepared using bacteria-free agar while $SS_{E.COLI}$ refers to bacterial biofilm).

The observed decrease in CPD of *E.coli* biofilm on 316L stainless steel along with the increase in incubation time can be explained as follows. Most bacteria (including *E. coli*) above their the whole-cell isoelectric point (IEP, which for most bacteria lays in the low pH range of 1.5-4.5), show a negative net charge, which in turn is related to the number of charged acidic and basic groups present in bacterial surface polymers and in their extracellular polymeric substances matrix [41]. Thus, as the number of *E.coli* bacteria and their colonies increased along with the biofilm incubation time the net negative charge of the biofilm also increased. In result, the CPD was shifted towards more negative values as the Kelvin probe reacts not only to variations in WF but it also identifies the charged state of the analyzed surface. Thus, the observed CPD decrease was more likely to be related to the change in the surface charge density (linked to the increasing number of bacteria on the examined surface) than to a change in the WF of the bacterial biofilm as a whole.

Moreover, even a low number of *E.coli* bacterial clusters (corresponding to ca. 0.6% of the specimen surface, as verified using SEM) formed during the initial 24-long breed period was detected by SKP. The additional benefit of using SKP method to detect and monitor bacterial *E. coli* biofilm development is related to its large (hundreds of mm^2) surface area analysis capabilities as compared to KPFM (offering µm-sized spans) and thus it may be applicable in scientific examinations of bacterial incursions in real objects like medical, personal care or amusement devices.

3.2 µFTIR

ATR-FTIR mapping has been used for chemical identification and distribution of materials on the steel substrates. One of the key advantages of ATR-FTIR spectroscopy is the ability to measure even very thin films in a relatively undisturbed way without the need of any specific sample preparation, which makes it a versatile tool for investigating biofilm development in situ [42]. Representative images of reference stainless steel and *E. coli* biofilm-covered specimens are presented in Figure 6. These maps clearly show that the reference area is free of organic matter, while bacteria cells are present in the biofilm specimen region. It could be concluded from the integrated intensity of the absorption band between 3050-2900 cm^{-1} assigned to vibrations of CH_2 and CH_3 groups, which is substantially higher for bacteria spectra. In accordance with the obtained spectral maps (Figure 6 B-D), the distribution of bacteria single-cells is not uniform and cells clusters are present.

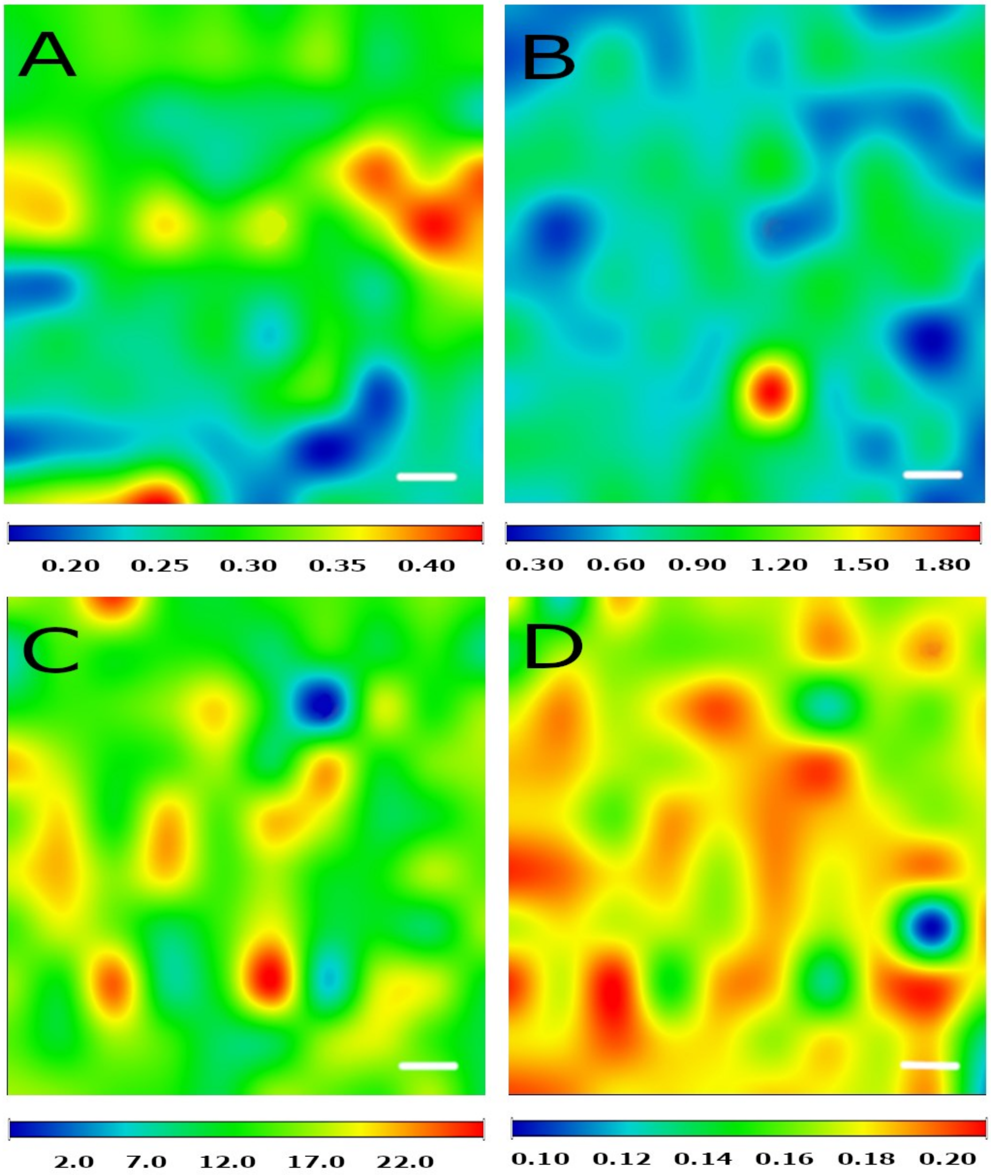

Figure 6. Representative ATR-FTIR mappings. **Upper:** The distribution of organic matter in analyzed areas by integrating the CH_2 stretching band at 2920 cm^{-1} in the ATR-FTIR spectrum (3000-2800 cm^{-1}): (**A)** - reference stainless steel specimen, (**B)** - E. coli biofilm-covered specimen. **Bottom**: The distribution of proteins from integration of Amide I band area (1700-1600 cm^{-1}) (**C**) and lipids based on integration of the carbonyl band ν(C=O) at 1735 cm^{-1} (**D**) in bacteria specimen area. **White scale bar:** 50 μm.

The average spectrum shown in Figure 7. identifies the presence of inorganic impurities (corundum and silica carbide) on the stainless-steel surface in bacteria-free specimen region. A very weak band at around 1260 cm^{-1} corresponds to $–Si(CH_3)$ and a weak broad band at 1100 cm^{-1} can be assigned to –Si–O–Si– and Al-O-Si groups [43], which leads to a conclusion that these are sandpaper and siloxane adhesive residues.

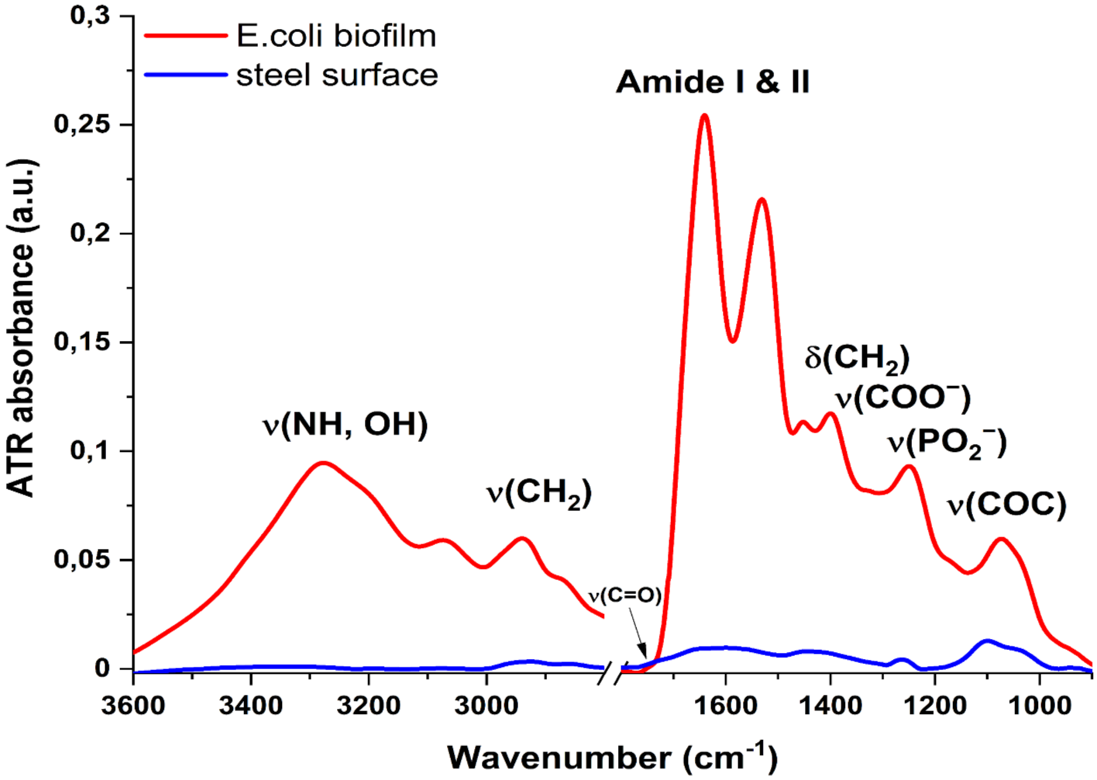

Figure 7. Average ATR-FTIR spectra of analyzed areas (blue line: bacteria-free specimen region, red line: *E. coli* biofilm-covered specimen region).

In turn, the average spectrum obtained for the steel surface covered with bacteria, shown in Figure 7 is typical for *Escherichia coli* strains [44,45] and it is dominated by the absorption of proteins and lipid membrane constituents [22,46,47]. The most intensive is Amide I band at 1640 cm^{-1}, which is mainly corresponding to the stretching vibration v(C=O) carbonyl groups of the peptide bond. In addition, in bacteria infrared spectra in the wavenumber range of 1300-1200 cm^{-1} nucleic acids bands are observed, on the other hand, in the 1200-950 cm^{-1} region an absorption from carbohydrates occurs. The complex band at 1074 cm^{-1} can be mainly assigned to the C-O-C glycosidic linkage and C-O-C stretching of carbohydrates in bacterial cell walls, as well as to the stretching vibrations of PO_2^- groups in phospholipids and nucleic acids. The weak shoulder band at ~1745 cm^{-1} originates from stretching vibrations of ester carbonyl groups (C=O) is related to lipoproteins and phospholipids. This band is considered to be a marker of EPS (extracellular polymeric substances) [46,48]. The presence of the intensive and broad band at 3400 cm^{-1} mostly arising from stretching vibrations of OH groups in water molecules is the proof that the bacteria cells contained in the analyzed biofilm stayed in hydrated, probably viable form.

3.3 DHT examination

The DHT was used for detection of the formation of bacterial biofilm on the glass-surface without the presence of any nutrients by reconstructed 3D-RI distributions. The average length and width of the adult (non-dividing) *E. coli* cells on glass-surface was equal to 2.8 μm and 1.2 μm, respectively. Obtained results indicated that the *E. coli* cells cultivated on this surface have larger spatial size than cells cultivated on steel-surface during the SEM examination, what may be related with the cells' dehydration process necessary for SEM imaging.

However, during the cell division, the bacteria cell is changing its morphology and RI-values. Generally, cell division (or cytokinesis) is one of the fundamental processes enabling the proliferation of both prokaryotic and eukaryotic cells. Cytokinesis is induced by a complex of proteins that constitute the division apparatus [49]. This process is spatially and temporarily correlated with other cell processes as: DNA replication (duplication of the genetic material), segregation of nucleoids and cytoplasm (their distribution between two cells), generation of the septum between two cells and the final separation of cells' walls and membranes. The RI value of cell cytoplasm is linearly related to its protein concentration, local protein concentration of a cell [50] associated with the DNA replication and the segregation of the nucleoids can be retrieved from RI-data. Moreover, the initial (parent) cell prepares for division by enlarging the cell wall, cell membrane and overall volume, what leads to the changes of the cell morphology which can be also retrieved from reconstructed RI-data. Therefore, it was necessary to analyze the variation of RI-values during this physiological process to include in our examination also such kinds of cells. Representative and exemplary results related with cell division are shown on Figure 8. Initially, the bacteria cell has uniform distribution of the cytoplasm inside the cell (Figure 8A) and the local maxima of RI-values representing the local increase of the protein's concentration related with the location of the nucleoids and ribosomes are present. When the cells division is beginning the *E. coli* cell's size is increased.

Moreover, the local concentration of the proteins inside the cell can be observed (see Figure 8 B).

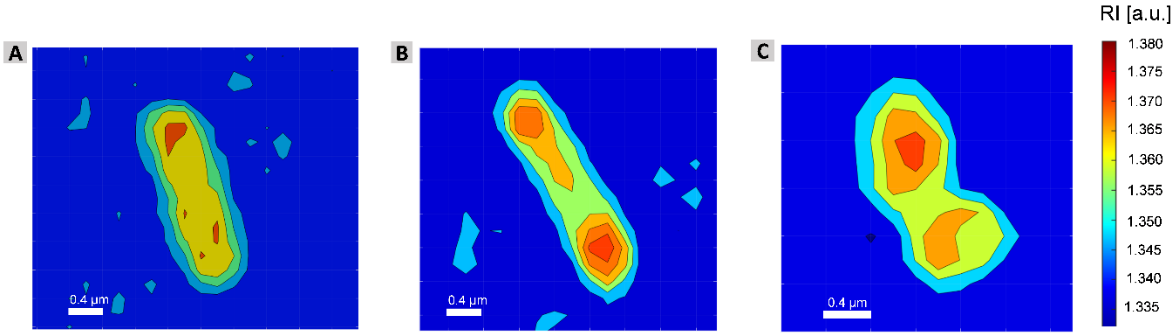

Figure 8. The representative 2D-RI tomograms of the initial *E. coli* single-cell before cell division (**A**), after DNA replication and segregation of nucleoids (**B**) and during septum synthetization (**C**).

It is related with the local increase of the RI-values at the opposite ends of cell revealed segregation of the nucleoids and cytoplasm following the DNA replication. The synthetization of the septum in the cell center is indicated by the decrease of the cell diameter in the central region (see Figure 8 C).

Based on the representative 2D-RI tomograms, the range of RI-values' variation between the dividing cells and already divided cells was determined to visualize all cells present on the examined glass-surface. It was shown that the range of RI-values' variation between analyzed cells is from 1.345 to 1.380 (see Figure 8). Obtained results are indicating that the spatial distribution of the RI-values is depending on the stage of the bacteria cells division and it is possible to characterize this process based on measured 2D/3D-RI tomograms. Furthermore, the existence of such variations of the RI-distribution indicates that the *E. coli* cells on the glass-surface without presence of any nutrients have the ability for cell division and multiplication. However, it should be pointed out that the RI-values and 2D-RI distribution is depending also on the kind of the surrounding medium and its RI-value [51] , therefore depending on the used procedures of sample's preparation, the determined RI-data can be different.

After determination of this RI-values' range inside the single cell, the digital staining was performed to visualize all bacteria cells on the glass-surface. The exemplary results are shown on Figure 9.

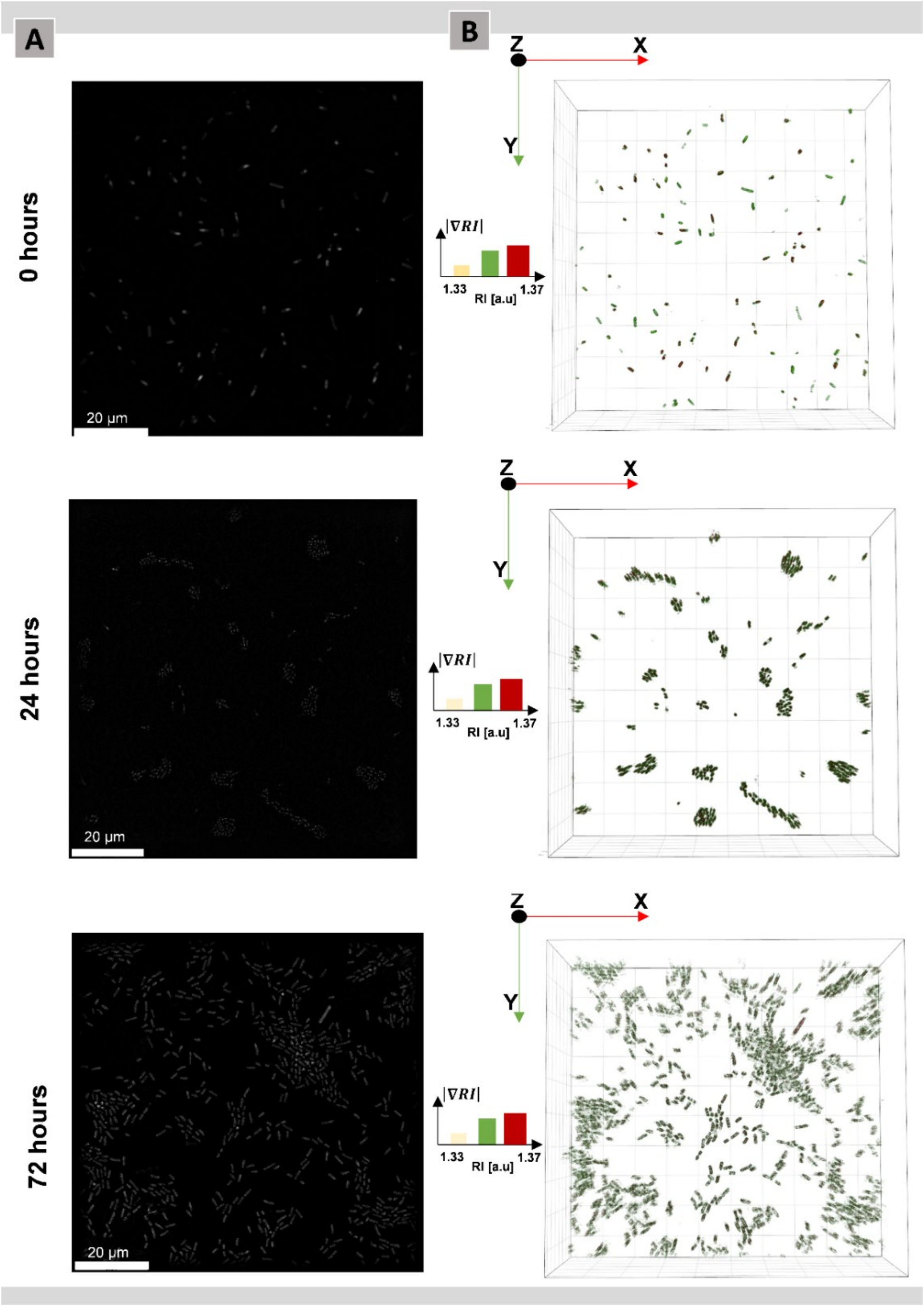

Figure 9. The representative results of the 2D-RI tomograms (**A**), reconstructed, rendered and digitally stained 3D-RI tomograms of *E. coli* cells (**B**) indicating the initial sample and the process of biofilm formation after 24 and 72 hours of cultivation.

It can be seen that after 24 hours the *E. coli* bacteria are able to biofilm formation on the glass-surface without the presence of nutrients as in case of the steel-surface. Moreover, the number of cells is still increased over time, which indicates that despite the lack of nutrients in the surrounding medium the living bacteria cells can still be able to divide on glass-surface. Moreover, the rendered 3D-RI tomograms demonstrated that on the analyzed surface the bacteria cells are forming the monolayer (see movie1 in Supplementary Materials).

3.4 The assessment of obtained results of multi-modal measurements

The food- and medical-grade 316L austenitic stainless steel was used in our biofilm-adhesion experiments as a substrate for Kelvin probe CPD examination while borosilicate glass was applied in DHT imaging. Both substrates have their unique but different properties (high electrical conductance versus strong dielectric character as well as differences in roughness and thus bacterial film affinity) and they represent medically relevant surfaces and standard engineering materials used in common products. Yet, both types of tested materials (glass and metal) as hydrophilic are less likely to be colonized by *E. coli* than e.g. plastics or other hydrophobic and non-polar surfaces, according to Beloin [52] and Donlan [53]. All experiments were also performed in temperature and humidity conditions closely approximating typical room conditions, thus bacterial growth was observed in every-day circumstances faced by medical and entertaining devices handled by humane users.

In all experiments, a scanning Kelvin probe with off-null detection was used to identify intact *E. coli* biofilms over a large area (50 mm^2) of the metallic samples. The relative standard error of the CPD values recorded for water-dipped 316L stainless steel substrates was below 0.7% and it was higher than the data variation (0.3%) recorded for Au reference used as the WF calibration surface however, such variation in CPD in real polycrystalline metallic surfaces are commonly observed. On the other hand, the relative standard error of the CPD measured for biofilm-covered 316L steel specimens was dependent on the biofilm cultivation time; while for 24 hours it was not higher than 2.0% yet for 72 hours-long cultivation, it was generally below 10% but a specimen with over 50% relative standard error was also discovered. This may indicate that the higher variation in CPD measurements observed in biofilms is related to the biofilm itself (its arbitrary geometry and random distribution of single cells and cells clusters) rather than to the Kelvin probe instrument. The *E. coli* cells and formed biofilms can exhibit the spatial heterogeneity related to the different locations of single-cells attachment to the surface and different process of the biofilm development, what may be responsible for higher statistical spread of the measurement results.

As summarized in Figure 4, *E. coli* biofilm cultivated for 24 hours has a substantially higher CPD value than that recorded for a biofilm cultivated for 72 hours. This is related to the bacterial film development, proliferation, and the corresponding increase in number of bacteria cells per surface unit, as illustrated on glass specimens by holotomographic imaging presented in Figure 9. As the goal of the presented research was to detect formation of living *E. coli* biofilms, the cells could not be dehydrated (dried) before holotomographic imaging and CPD scans thus, water adsorbed within the biofilms may interfere with the obtained results. This effect was observed in case of the SEM results, where the cells' dehydration led to the decrease of their size in comparison with the results of the DHT examination. The biofilm samples on glass and stainless-steel surfaces were prepared with the same manner, therefore the possible dehydration of bacteria cells has been excluded by the IR microscopy which confirmed the hydrated form of cells on stainless steel surface by the presence of the intensive and broad band at 3400 cm^{-1} mostly arising from stretching vibrations of OH groups in water molecules.

Our holotomographic observations (Fig.9) suggest that the *E. coli* cells are dividing and multiplexing easily and form a bacterial monolayer on glass surface. Another possible cause of the observed variations in CPD may be related to the changes of the bacteria cell size or their spatial reorientation during the biofilm development in time, when the concentration of bacteria cells in the biofilm and on the examined surfaces was increased. This was partially confirmed by the DHT examination, which demonstrated that during the cell division the individual parent cells exhibit the time-resolved morphological changes (including cell's size) and local changes of the protein's concentration related to the cytokinesis. Such process can be present also during CPD scans, even if the used surfaces in each examination were differing not only in its basic material composition but also in the roughness, which may modify the biofilm growth and its morphology. On the other hand, studies performed by Rodriguez suggests that the surface roughness is not significantly correlated with the *L. monocytogenes* attachment and biofilm formation on stainless steel [54] and similar observations not linking the biofilm growth rate with surface roughness were also reported by Percival for 316-grade stainless steel and bacterial flora commonly found in potable water (including *Acinetobacter sp, Pseudomonas* spp*, Methylobacterium* sp*, and Corynebacterium / Arthrobacter* spp) [55].

4. CONCLUSIONS

In summary, we have presented a novel multimode approach to a non-contact and label-free detection of the *E. coli* biofilm formation on the glass and stainless-steel surfaces. It was demonstrated that the synergistic analysis using selected techniques enables the multi-parametric characterization of bacterial biofilm formation on optically transparent and non-transparent as well as conductive and non-conductive surfaces. The here-proposed approach combines the chemical composition of bacterial biofilms with their electrical, optical, morphological properties. The method enables examination of the samples on larger scale, and can be easily adapted by conventional microbiological laboratories, where such samples are investigated on daily basis.

To analyze the non-transparent and conductive or semi-conductive samples as stainless steel, the KP, SEM and IR-microscopy was applied, and cross-examined using classical SEM microscopy. According to our knowledge this is the first attempt to examine biofilm formation by measuring the contact potential difference CPD distributions using scanning probe, as the available literature presents studies with nanometer resolution on single-cell level by means of KPFM. We investigated the CPD of *E. coli* bacterial biofilms deposited on food- and medical- 316L-grade stainless steel substrates under laboratory conditions closely mimicking those observed in everyday practice. The CPD of the metallic 316L stainless steel substrate covered with juvenile (24h old) *E. coli* biofilm changed significantly not only in comparison with the CPD of the stainless steel itself, but it was also experimentally proven that it increased over time as the biofilm was formed. This non-contact measurement technique can be used to develop and verify tests of the bacterial biofilm existence on common solid surfaces like stainless steel. The shape, dimensions, wettability, surface roughness, and CPD are all expected to play a critical role in determining the adhesion force between a bacterial biofilm and a planar substrate surface.

The IR-spectra confirmed that after 24 hours the biofilm formation on larger surfaces can be detected based on the presence of the characteristic bands of: CH_2 and CH_3 groups, Amide I, nucleic acids, carbohydrates in bacterial cell walls, or lipoproteins and phospholipids, considered to be a marker of extracellular polymeric substances which are responsible for adhesion of biofilms to surfaces.

On the other hand, in case of the optically transparent, conductive/non-conductive substrates, it was possible to use the DHT technique for analysis of the bacterial biofilm formation. This approach based on the reconstructed RI-data, provided the information about the local density and proteins changes inside the single-cells. Obtained results have shown, that also in case of the glass surfaces the *E. coli* bacteria are able to form a biofilm as observed for stainless steel. It was shown that the dehydration of cells during SEM is significantly affecting the cells' morphology. Moreover, it was demonstrated that this technique is suitable not only for visualization of single-cells and biofilm formation, but also the cytokinesis process and during the examination of the biofilm formation it is essential to take into consideration the fact, that at the same time, bacteria cells forming the biofilm can be at different stages of cell division and in consequence their morphology, proteins and cytoplasm concentration will be changing.

The proposed techniques can be applied for the multi-parametric detection and characterization of the biofilm formation and dynamics of this process on surfaces of the most common materials (optically transparent/non-transparent, conductive/semi-conductive or non-conductive) used in medical devices and instrumentation, but also others used in everyday life as mobile phones. The accurate identification and modeling of factors promoting bacterial cell adhesion and biofilm formation can prove extremely important in controlling the consequences of intentional or accidental bacterial surface contamination.

Funding

This research was fully funded by the National Center of Science, Poland, grant number 2021/41/B/ST7/04002.

References

[1] T.D. N, G. V K, A.E. O, Bacterial Contamination of Mobile Phones: When Your Mobile Phone Could Transmit More Than Just a Call, n.d. http://www.webmedcentral.comon (accessed April 29, 2021).

[2] U.V. Albrecht, U. Von Jan, L. Sedlacek, S. Groos, S. Suerbaum, R.P. Vonberg, Standardized, app-based disinfection of ipads in a clinical and nonclinical setting: Comparative analysis, J. Med. Internet Res. 15 (2013) e2643.

https://doi.org/10.2196/jmir.2643.

[3] F. Zhou, T. Yu, R. Du, G. Fan, Y. Liu, Z. Liu, J. Xiang, Y. Wang, B. Song, X. Gu, L. Guan, Y. Wei, H. Li, X. Wu, J. Xu, S. Tu, Y. Zhang, H. Chen, B. Cao, Clinical course and risk factors for mortality of adult inpatients with COVID-19 in Wuhan, China: a retrospective cohort study, Lancet. 395 (2020) 1054–1062. https://doi.org/10.1016/S0140-6736(20)30566-3.

[4] Welcome to Accu-Chek.co.uk, (n.d.). https://www.accu-chek.co.uk/ (accessed April 29, 2021).

[5] Selected EPA-Registered Disinfectants | Pesticide Registration | US EPA, (n.d.). https://www.epa.gov/pesticide-registration/selected-epa-registered-disinfectants (accessed April 29, 2021).

[6] WHO | WHO guidelines on hand hygiene in health care, (n.d.). https://www.who.int/infection-prevention/publications/hand-hygiene-2009/en/ (accessed April 29, 2021).

[7] J. Morvai, R. Szabó, The role of mobile communication devices in the spread of infections, Orv. Hetil. 156 (2015) 802–807. https://doi.org/10.1556/650.2015.30147.

[8] M. Olsen, M. Campos, A. Lohning, P. Jones, J. Legget, A. Bannach-Brown, S. McKirdy, R. Alghafri, L. Tajouri, Mobile phones represent a pathway for microbial transmission: A scoping review, Travel Med. Infect. Dis. 35 (2020) 101704. https://doi.org/10.1016/j.tmaid.2020.101704.

[9] R.I. Mackie, A. Sghir, H.R. Gaskins, Developmental microbial ecology of the neonatal gastrointestinal tract, Am. J. Clin. Nutr. 69 (1999) 1035s-1045s. https://doi.org/10.1093/ajcn/69.5.1035s.

[10] Lord Kelvin, V. Contact electricity of metals , London, Edinburgh, Dublin Philos. Mag. J. Sci. 46 (1898) 82–120. https://doi.org/10.1080/14786449808621172.

[11] W.A. Zisman, A new method of measuring contact potential differences in metals, Rev. Sci. Instrum. 3 (1932) 367–370. https://doi.org/10.1063/1.1748947.

[12] G.N. Derry, M.E. Kern, E.H. Worth, Recommended values of clean metal surface work functions, J. Vac. Sci. Technol. A Vacuum, Surfaces, Film. 33 (2015) 060801. https://doi.org/10.1116/1.4934685.

[13] N. Barrett, O. Renault, H. Lemaître, P. Bonnaillie, F. Barcelo, F. Miserque, M. Wang, C. Corbel, Microscopic work function anisotropy and surface chemistry of 316L stainless steel using photoelectron emission microscopy, J. Electron Spectros. Relat. Phenomena. 195 (2014) 117–124. https://doi.org/10.1016/j.elspec.2014.05.015.

[14] A.C. Ahn, B.J. Gow, R.G. Martinsen, M. Zhao, A.J. Grodzinsky, I.D. Baikie, Applying the Kelvin probe to biological tissues: Theoretical and computational

analyses, Phys. Rev. E - Stat. Nonlinear, Soft Matter Phys. 85 (2012) 061901. https://doi.org/10.1103/PhysRevE.85.061901.

[15] J. Colchero, A. Gil, A.M. Baró, Resolution enhancement and improved data interpretation in electrostatic force microscopy, Phys. Rev. B - Condens. Matter Mater. Phys. 64 (2001) 245403. https://doi.org/10.1103/PhysRevB.64.245403.

[16] E. Birkenhauer, S. Neethirajan, Characterization of electrical surface properties of mono- and co-cultures of Pseudomonas aeruginosa and methicillin-resistant Staphylococcus aureus using Kelvin probe force microscopy, RSC Adv. 4 (2014) 42432–42440. https://doi.org/10.1039/c4ra07446g.

[17] I. Lee, E. Chung, H. Kweon, S. Yiacoumi, C. Tsouris, Scanning surface potential microscopy of spore adhesion on surfaces, Colloids Surfaces B Biointerfaces. 92 (2012) 271–276. https://doi.org/10.1016/j.colsurfb.2011.11.052.

[18] M. Gultekinoglu, Y.J. Oh, P. Hinterdorfer, M. Duman, D. Çatçat, K. Ulubayram, Nanoscale characteristics of antibacterial cationic polymeric brushes and single bacterium interactions probed by force microscopy, RSC Adv. 6 (2016) 17092–17099. https://doi.org/10.1039/c5ra22434a.

[19] V. Erukhimovitch, V. Pavlov, M. Talyshinsky, Y. Souprun, M. Huleihel, FTIR microscopy as a method for identification of bacterial and fungal infections, J. Pharm. Biomed. Anal. 37 (2005) 1105–1108. https://doi.org/10.1016/j.jpba.2004.08.010.

[20] D. Naumann, Infrared Spectroscopy in Microbiology, Encycl. Anal. Chem. (2006) 1–29. https://doi.org/10.1002/9780470027318.a0117.

[21] M.I. Santos, E. Gerbino, E. Tymczyszyn, A. Gomez-Zavaglia, Applications of infrared and raman spectroscopies to probiotic investigation, Foods. 4 (2015) 283–305. https://doi.org/10.3390/foods4030283.

[22] B. Gieroba, M. Krysa, K. Wojtowicz, A. Wiater, M. Pleszczyńska, M. Tomczyk, A. Sroka-Bartnicka, The FT-IR and raman spectroscopies as tools for biofilm characterization created by cariogenic streptococci, Int. J. Mol. Sci. 21 (2020) 1–20. https://doi.org/10.3390/ijms21113811.

[23] H.Y. Cheung, G.K.L. Chan, S.H. Cheung, S.Q. Sun, W.F. Fong, Morphological and chemical changes in the attached cells of Pseudomonas aeruginosa as primary biofilms develop on aluminium and CaF2 plates, J. Appl. Microbiol. 102 (2007) 701–710. https://doi.org/10.1111/j.1365-2672.2006.03137.x.

[24] H. Yang, F. Wu, F. Xu, K. Tang, C. Ding, H. Shi, S. Yu, Bacterial Typing and Identification Based on Fourier Transform Infrared Spectroscopy, (2020) 1–58. https://doi.org/10.21203/rs.2.23337/v1.

[25] R. Davis, A. Deering, Y. Burgula, L.J. Mauer, B.L. Reuhs, Differentiation of

live, dead and treated cells of Escherichia coli O157: H7 using FT-IR spectroscopy, J. Appl. Microbiol. 112 (2012) 743–751. https://doi.org/10.1111/j.1365-2672.2011.05215.x.

[26] A. Kuś, W. Krauze, M. Kujawińska, Active limited-angle tomographic phase microscope, J. Biomed. Opt. 20 (2015) 1. https://doi.org/10.1117/1.JBO.20.11.111216.

[27] A. Kuś, W. Krauze, M. Kujawińska, Limited-angle holographic tomography with optically controlled projection generation, in: T.G. Brown, C.J. Cogswell, T. Wilson (Eds.), Three-Dimensional Multidimens. Microsc. Image Acquis. Process. XXII, SPIE, 2015: p. 933007. https://doi.org/10.1117/12.2078111.

[28] Y. Baek, Y. Park, Intensity-based holographic imaging via space-domain Kramers–Kronig relations, Nat. Photonics. (2021). https://doi.org/10.1038/s41566-021-00760-8.

[29] Y. Cotte, F. Toy, P. Jourdain, N. Pavillon, D. Boss, P. Magistretti, P. Marquet, C. Depeursinge, Marker-free phase nanoscopy, Nat. Photonics. 7 (2013) 113–117. https://doi.org/10.1038/nphoton.2012.329.

[30] A.K. Singh, L. Leprun, R. Drolia, X. Bai, H. Kim, A. Aroonnual, E. Bae, K.K. Mishra, A.K. Bhunia, Virulence gene-associated mutant bacterial colonies generate differentiating two-dimensional laser scatter fingerprints, Appl. Environ. Microbiol. 82 (2016). https://doi.org/10.1128/AEM.04129-15.

[31] S.E. Koo, S. Jang, Y.K. Park, C.J. Park, Reconstructed three-dimensional images and parameters of individual erythrocytes using optical diffraction tomography microscopy, Ann. Lab. Med. 39 (2019) 223–226. https://doi.org/10.3343/alm.2019.39.2.223.

[32] Y. Wang, W. Shang, H. Zhong, T. Luo, M. Niu, K. Xu, J. Tian, Tumor vessel targeted self-assemble nanoparticles for amplification and prediction of the embolization effect in hepatocellular carcinoma, ACS Nano. 14 (2020) 14907–14918. https://doi.org/10.1021/acsnano.0c04341.

[33] T.-K. Kim, B.-W. Lee, F. Fujii, K.-H. Lee, S. Lee, Y. Park, J.K. Kim, S.-W. Lee, C.-G. Pack, Mitotic Chromosomes in Live Cells Characterized Using High-Speed and Label-Free Optical Diffraction Tomography, Cells. 8 (2019) 1368. https://doi.org/10.3390/cells8111368.

[34] R.P. Friedrich, E. Schreiber, R. Tietze, H. Yang, C. Pilarsky, C. Alexiou, <p>Intracellular Quantification and Localization of Label-Free Iron Oxide Nanoparticles by Holotomographic Microscopy</p>, Nanotechnol. Sci. Appl. Volume 13 (2020) 119–130. https://doi.org/10.2147/NSA.S282204.

[35] S.A. Yang, J. Yoon, K. Kim, Y.K. Park, Measurements of morphological and biophysical alterations in individual neuron cells associated with early neurotoxic effects in Parkinson’s disease, Cytom. Part A. 91 (2017) 510–518. https://doi.org/10.1002/cyto.a.23110.

[36] S. Gutbier, F. Wanke, N. Dahm, A. Rümmelin, S. Zimmermann, K. Christensen, F. Köchl, A. Rautanen, K. Hatje, B. Geering, J.D. Zhang, M. Britschgi, S.A. Cowley, C. Patsch, Large-Scale Production of Human iPSC-Derived Macrophages for Drug Screening, Int. J. Mol. Sci. 21 (2020) 4808. https://doi.org/10.3390/ijms21134808.

[37] A. Savitzky, M.J.E. Golay, Smoothing and Differentiation of Data by Simplified Least Squares Procedures, Anal. Chem. 36 (1964) 1627–1639. https://doi.org/10.1021/ac60214a047.

[38] Y. Cheng, G. Feng, C.I. Moraru, Micro- and Nanotopography Sensitive Bacterial Attachment Mechanisms : A Review, 10 (2019) 1–17. https://doi.org/10.3389/fmicb.2019.00191.

[39] C.S. Alves, M.N. Melo, H.G. Franquelim, R. Ferre, M. Planas, L. Feliu, E. Bardají, W. Kowalczyk, D. Andreu, N.C. Santos, M.X. Fernandes, M.A.R.B. Castanho, Escherichia coli cell surface perturbation and disruption induced by antimicrobial peptides BP100 and pepR, J. Biol. Chem. 285 (2010) 27536–27544. https://doi.org/10.1074/jbc.M110.130955.

[40] D.H. Abdeen, M.A. Atieh, B. Merzougui, W. Khalfaoui, Corrosion Evaluation of 316L Stainless Steel in CNT-Water Nanofluid: Effect of CNTs Loading, Materials (Basel). 12 (2019) 1634. https://doi.org/10.3390/ma12101634.

[41] B.A. Jucker, H. Harms, A.J.B. Zehnder, Adhesion of the positively charged bacterium Stenotrophomonas (Xanthomonas) maltophilia 70401 to glass and teflon, J. Bacteriol. 178 (1996) 5472–5479. https://doi.org/10.1128/jb.178.18.5472-5479.1996.

[42] J. Schmitt, H.C. Flemming, FTIR-spectroscopy in microbial and material analysis, Int. Biodeterior. Biodegrad. 41 (1998) 1–11. https://doi.org/10.1016/S0964-8305(98)80002-4.

[43] W.K.W. Lee, J.S.J. Van Deventer, Use of Infrared Spectroscopy to Study Geopolymerization of Heterogeneous Amorphous Aluminosilicates, Langmuir. 19 (2003) 8726–8734. https://doi.org/10.1021/la026127e.

[44] Ł. Lechowicz, W. Adamus-Białek, W. Kaca, Attenuated total reflectance fourier transform infrared spectroscopy and artificial neural networks applied to differentiate Escherichia coli papG +/ papG- strains, J. Spectrosc. 1 (2013). https://doi.org/10.1155/2013/538686.

[45] P. Stenclova, S. Freisinger, H. Barth, A. Kromka, B. Mizaikoff, Cyclic Changes in the Amide Bands Within Escherichia coli Biofilms Monitored Using Real-Time Infrared Attenuated Total Reflection Spectroscopy (IR-ATR), Appl. Spectrosc. 73 (2019) 424–432. https://doi.org/10.1177/0003702819829081.

[46] M.S.I. Khan, E.J. Lee, Y.J. Kim, A submerged dielectric barrier discharge plasma inactivation mechanism of biofilms produced by Escherichia coli O157:H7, Cronobacter sakazakii, and Staphylococcus aureus, Sci. Rep. 6 (2016) 1–11. https://doi.org/10.1038/srep37072.

[47] J. Soler-Arango, C. Figoli, G. Muraca, A. Bosch, G. Brelles-Mariño, The Pseudomonas aeruginosa biofilm matrix and cells are drastically impacted by gas discharge plasma treatment: A comprehensive model explaining plasma-mediated biofilm eradication, PLoS One. 14 (2019) 1–27. https://doi.org/10.1371/journal.pone.0216817.

[48] K. Kochan, D. Perez-Guaita, J. Pissang, J.H. Jiang, A.Y. Peleg, D. McNaughton, P. Heraud, B.R. Wood, In vivo atomic force microscopy-infrared spectroscopy of bacteria, J. R. Soc. Interface. 15 (2018). https://doi.org/10.1098/rsif.2018.0115.

[49] A.D. Vedyaykin, E. V. Ponomareva, M.A. Khodorkovskii, S.N. Borchsenius, I.E. Vishnyakov, Mechanisms of Bacterial Cell Division, Microbiol. (Russian Fed. 88 (2019) 245–260. https://doi.org/10.1134/S0026261719030159.

[50] G. Popescu, Y.K. Park, N. Lue, C. Best-Popescu, L. Deflores, R.R. Dasari, M.S. Feld, K. Badizadegan, Optical imaging of cell mass and growth dynamics, Am. J. Physiol. - Cell Physiol. 295 (2008) 538–544. https://doi.org/10.1152/ajpcell.00121.2008.

[51] M. Baczewska, K. Eder, S. Ketelhut, B. Kemper, M. Kujawińska, Refractive Index Changes of Cells and Cellular Compartments Upon Paraformaldehyde Fixation Acquired by Tomographic Phase Microscopy, Cytom. Part A. (2020) cyto.a.24229. https://doi.org/10.1002/cyto.a.24229.

[52] C. Beloin, A. Roux, J.M. Ghigo, Escherichia coli biofilms, Curr. Top. Microbiol. Immunol. 322 (2008) 249–289. https://doi.org/10.1007/978-3-540-75418-3_12.

[53] R.M. Donlan, Biofilms: Microbial life on surfaces, Emerg. Infect. Dis. 8 (2002) 881–890. https://doi.org/10.3201/eid0809.020063.

[54] A. Rodriguez, W.R. Autio, L.A. McLandsborough, Effect of surface roughness and stainless steel finish on Listeria monocytogenes attachment and biofilm formation, J. Food Prot. 71 (2008) 170–175. https://doi.org/10.4315/0362-028X-71.1.170.

[55] S.L. Percival, J.S. Knapp, D.S. Wales, R.G.J. Edyvean, The effect of turbulent flow and surface roughness on biofilm formation in drinking water, J. Ind. Microbiol. Biotechnol. 22 (1999) 152–159. https://doi.org/10.1038/sj.jim.2900622.